Use of radiochromic films for the absolute dose evaluation in high dose-rate proton beams

G.A.P. Cirrone,[a,b] **G. Petringa,**[a,1] **B.M. Cagni,**[a] **G. Cuttone,**[a] **G.F. Fustaino,**[a] **M. Guarrera,**[a] **R. Khanna**[a] **and R. Catalano**[a]

[a]*INFN-LNS (Italian Institute for Nuclear Physics),*
Via S Sofia 62, Catania, Italy

[b]*Physics and Astronomy Department, University of Catania,*
Via S Sofia 64, Catania, Italy

E-mail: giada.petringa@lns.infn.it

Abstract: Dosimetry of high dose-rate charged particle beams is becoming an important topic in radiation physics, especially after the advent of particle beams generated in the laser-matter interaction and of the experimental evidence of their clinical advantage on healthy tissues sparing. In this work, the use of radiochromic films as detector for absolute dosimetry of high rates proton beams is discussed.

2020 JINST 15 C04029

---

[1]Corresponding author.

Contents

1 Introduction

Over the last decades, charged particle acceleration using ultra-intense and ultra-short laser pulses has become one of the most attractive topics in relativistic laser-plasma interaction research [1, 2] as well as in the field of acceleration physics. Laser accelerated particle beams show very peculiar characteristics; one of the most interesting being their extremely high dose rate that can easily reach the values of $10^6 - 10^7$ Gy per second.

The development of new acceleration schemes where the final dose rates easily reach the value of 40 Gy/sec or more, is today of great interest as potentially applicable to the emerging and more effective radiotherapy modality called flash radiotherapy. The release of ultra-high dose-rates seems to protect healthy tissues more than conventional radiotherapy, with the same damage to tumor tissues [3]; it is precisely in this experimental evidence that the advantage of flash radiotherapy can be understood. An important aspect of flash radiotherapy lies in the acceleration and transmission of the beam: while for conventional radiotherapy (electrons and photons) linear accelerators are used, such as LINAC [4], for charged particles cyclotrons and synchrotrons are used and of these, only the first can supply dose rates high enough to carry studies in the field of flash radiotherapy [5]. Therefore, in the field of charged particle therapy, new methods of acceleration are being sought to obtain greater beam intensities. Among these, the use of high power laser-matter interaction is one of the most promising. The growing interest towards these extremely high dose-rate beams is consequently leading to the development of new approaches to performing an

accurate and reliable absolute dosimetry. The response of detectors to be used with flash beams must be dose-rate independent and/or must permit a reliable and precise correction of their output. Different authors proposed the use of the Faraday Cup detector [6, 7] eventually coupled with multi-gap in-transmission ionization chambers [8] to perform on-line absolute dose evaluation at the irradiation point. Contemporarily, relative and absolute dosimetry with passive detectors can offer essential and complementary information, as the reconstruction of the particle energy spectra at the Faraday Cup entrance or absolute dose intercomparisons among the many passive detectors susceptible to be used in high dose-rate beams we must consider the radiochromic films (or RCF) detectors; they show high spatial resolution and contain an active layer that undergoes a polymerization process when they are crossed by ionizing radiation [9], the etching detectors (as CR39), based on polyal-diglycol-carbonate and suffering damage to their polymeric structure when hit by charged particles [10], and thermoluminescence dosimeters (TLD), exploiting the thermoluminescent properties of magnesium, copper and phosphorus-doped lithium fluoride crystals (LiF: Mg, Cu, P) [11]. These passive dosimeters each require a different reading process and an appropriate calibration against absolute dosimeters [9, 12–14]. In this work, we discuss the potential use of radiochromic films, model EBT3, for dosimetric and spectroscopic applications of high dose-rate proton beams generated in laser-matter interaction.

2 Material

2.1 Radiochromic films

Radiochromic is a type of self-developing film typically used in the testing and characterization of radiographic equipments such as CT scanners and radiotherapy linacs. They are based on the radiochromic reactions that represent a direct coloration of a media by the absorption of radiation, which does not require any latent thermal, optical or chemical development or amplification [15–17]. In more recent years, the use of radiochromic materials in the form of films has become widely used as dosimeters for industrial and medical applications. These dosimeters are mainly hydrophobic-substituted triphenylmethane leucocyanides that undergo a heterolytic bond scission of the nitrile group, which forms a highly colored dye salt in solid polymeric solution when irradiated. These molecules require a host material for film development, which normally consists of a storyline-, vinyl- or nylon-based polymer. The first models of radiochromic do however require large doses to deliver a distinguishable change in color, typically in the order of 10^4–10^6 Gy. A more recent film based on polydiacetylene has found extensive use in medical applications where low doses are required to be measured. These latter types of films, in fact, are supplied in various forms to match the specific need in medical dosimetry with dosimetric ranges from 2500 Gy down to 0.1 Gy, if required. The radiochromic EBT3 model is studied and characterized in this paper. EBT3, manufactured by Ashland Global Specialty Chemicals Inc., come in light-shielded boxes, each containing twenty-five sheets (20.3×25.4 cm^2). Each film is comprised of an active layer, around 28 μm thick, sandwiched between two 125 μm matte-polyester substrates. The active layer contains the active component, stabilizers amongst other components. The thickness of the active layer will slightly vary between different production lots.

2.2 Irradiation set-up

EBT3 irradiations are performed cutting a single foil in smaller squares, 3×3 cm^2 in dimension, perfectly fitting a Teflon holder specifically designed for the detectors' positioning (figure 1). It permits the irradiation of both, a single radiochromic foil or a group of them, packed in a stack configuration. In the latter, EBT3 foils are piled and pressed together, in order to avoid any air gap in between, by a set of screws. The stack configuration is adopted for the depth dose distribution curves and energy spectra reconstruction. The holder also permits the insertion of plastic slabs of calibrated thickness and it is equipped with reference points for its easy and reliable positioning along the beamline.
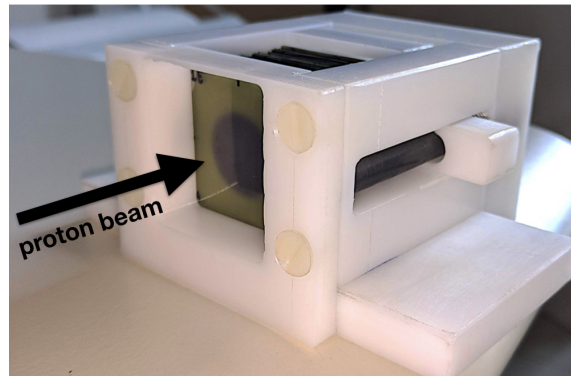
Figure 1. Teflon RCF holder containing a set of EBT films in stack configuration after proton irradiation. The proton beam entering from the left and its image, as a circular spot, are also visible.

All the irradiations were performed using three different proton beams configurations: two monochromatic (62 MeV and 30 MeV) beams and a clinical, modulated in energy, spread-out Bragg peak (SOBP). These beams were accelerated at the CATANA (Centro di AdroTerapia e Applicazioni Nucleari Avanzate) [18–20] eye proton therapy facility of the Italian Institute for Nuclear Physics in Catania, Italy. The details of the CATANA irradiation beamline transport elements and detectors together with the absolute and relative dosimetric procedures and associated uncertainties are described elsewhere [18, 19]. The proton beam calibration, in terms of absolute dose in water, is performed just before each irradiation in order to reduce the overall uncertainty; the variation of beam calibration on the various performed experiments resulted to be within 3%.

3 Methods

3.1 Dose calibration procedure

The RCFs were firstly calibrated in terms of absorbed dose in water. Calibration was performed irradiating different films of the same foil at different known doses in the range between 1 Gy to 20 Gy. In each irradiation, the film was positioned at the isocenter, in the same point where absolute dosimetry was previously carried out: at the proton Bragg peak entrance for the monochromatic cases (30 MeV and 60 MeV) and in the middle of the SOBP, for the clinically modulated one. As the polymerization process increases with the time, reaching a final, stable value after 24 hours, each film was read after this time period with an EPSON Expression Photo scanner, Model 10000

XL. The red channel and a resolution of 169 μm were chosen as the main parameters for imaging, as recommended by the EBT3 datasheet [21]. The film response, that must be correlated to the absorbed dose, is expressed in terms of film optical density (or OD). OD is a measure of the light transmittance and is conventionally defined as:

$$OD = -\log \frac{I}{I_0} \tag{3.1}$$

Here, I_0 represents the film background, measured as the average of a set of pixels values acquired in a non-irradiated section of the film; I is the average pixels' values in a region of interest (or ROI) corresponding to the homogeneous irradiated section of the film (figure 2).
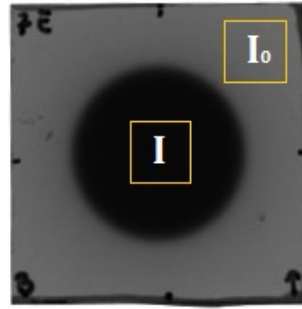
Figure 2. Image of and RCF irradiated with the two regions chosen for the I and I_0 estimation.

The dose calibration curve was obtained plotting the released dose D as a function of the resulting film optical density, as expressed in (3.1). The obtained calibration curve was then fitted with appropriate analytical functions that will be then used for dose reconstruction in different conditions. Three different analytical functions were chosen:

$$D_{\text{fit}}^{\text{3rd order polynomial}} = p_1 \cdot OD^3 + p_2 \cdot OD^2 + p_3 \cdot OD + p_4 \tag{3.2}$$

$$D_{\text{fit}}^{\text{exponential}} = p_1 \cdot e^{-OD \cdot p_2} + p_3 \tag{3.3}$$

$$D_{\text{fit}}^{\text{Double exponential}} = p1 \cdot e^{p_2 \cdot OD} + p_3 \cdot e^{p_4 \cdot OD} + p_5 \tag{3.4}$$

We hence generated three different calibration curves for each beam configuration. Each curve was statistically evaluated in order to verify, or eventually reject, the agreement with the corresponding experimental calibration.

3.2 Errors evaluations in the radiochromic reading procedure

The uncertainties associated with a measured optical density, as derived from (3.1), must be evaluated as directly affecting the calibration curves and, consequently, the energy spectra and the final dose distributions.

Uncertainties on I and I_0 can be expressed as the standard deviation of the pixel values contained in the ROI over which the I_0 and I values are estimated [9]. The one provided by the reading process estimated at around 2% of the value must be added. The ROI dimension and its position with respect to the beam axis were kept constant in each film reading in order to minimize the errors related to unlikely beam profile inhomogeneities. Once the uncertainty on I and I_0 was estimated,

it has to be propagated on the final value of OD. The error obtained on the OD must, in turn, be propagated, together with the errors on the fit parameters, to obtain the final error on the dose.

4 Results

4.1 Absolute dose calibration

Calibration curves were measured by irradiating radiochromic films at the entrance of a monochromatic 30 MeV and 60 MeV proton Bragg peak and at the middle of a 60 MeV clinical proton SOBP; all films belonged to the same production batch. Each calibration curve was hence fitted with three different analytical functions as generally recommended by literature [22, 23].
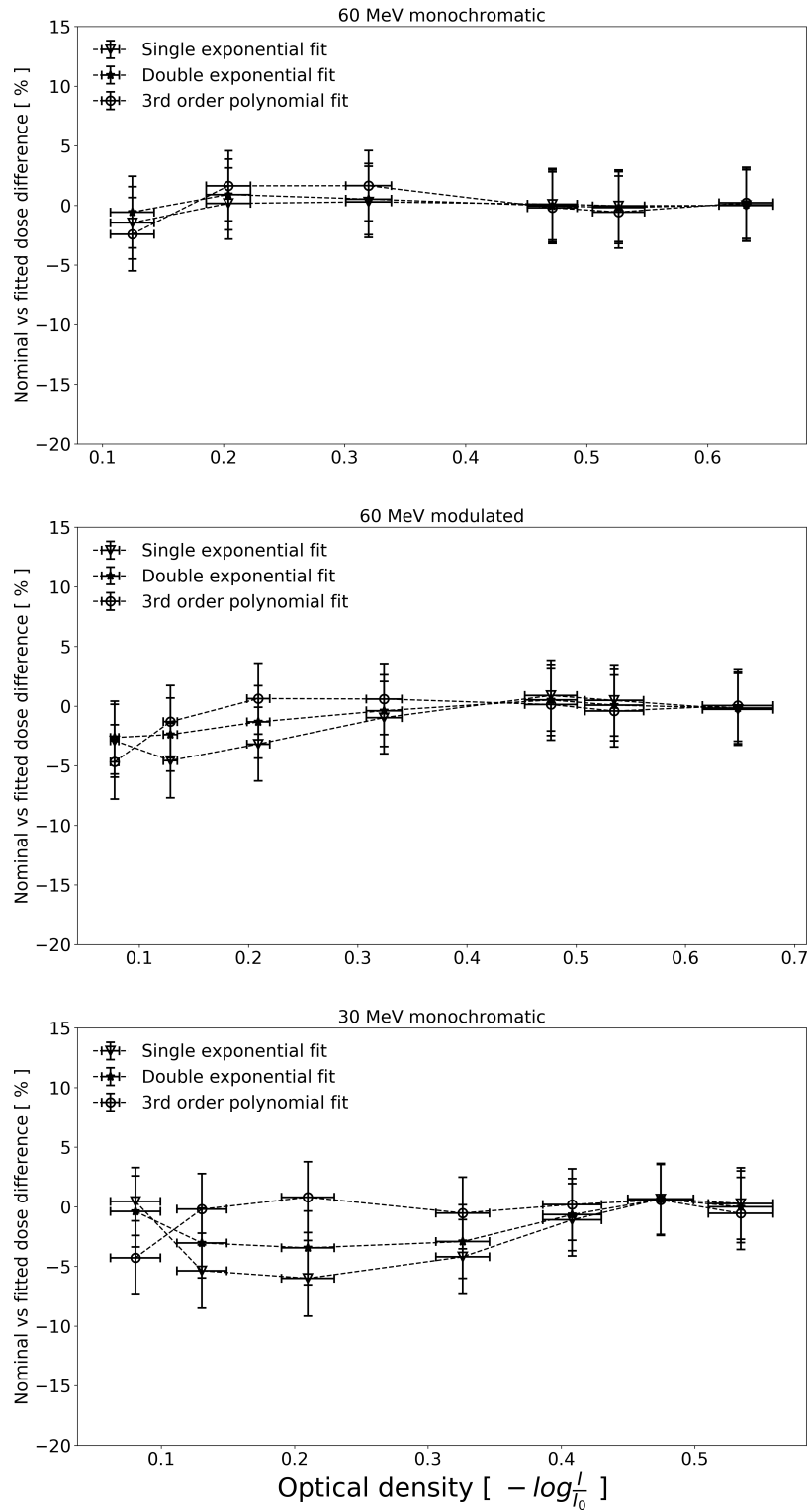
Figure 3 shows, for the three irradiation conditions, the percentage discrepancy between the experimental calibration curve and the three fit methods. Error bars for the percentage differences are calculated propagating the errors: a total standard deviation of 3% is assumed for the nominal released absolute dose while the error on the fitted points is derived from the fitted parameters and calculated with the Origin software. The considered dose ranges were 1 Gy – 15 Gy, 0.5 Gy – 15 Gy and 0.5 Gy – 20 Gy for the monochromatic 60 MeV, modulated 60 MeV and monochromatic 30 MeV beams, respectively. A larger discrepancy is found at the lowest dose for all cases, where the fit curve always overestimates the dose. This is a direct consequence of the fact that the fit minimization is performed not imposing the passage of data in the cartesian origin as we preferred not to introduce an additional constraint on the whole procedure. All discrepancies resulted to be less than 5%.

The agreement between each experimental curve and the three corresponding fits was evaluated using a non-parametric Kolmogorov-Smirnov (K-S) test for the case of two independent distributions [24]; the results are summarised in table 1 where the chosen fit function, the K-S statistical parameter (m*n*Dn,m), the corresponding p-value, and final test results are reported. Here m and n are the degrees of freedom of the test, corresponding to the number of samples of the two compared distributions.

Table 1. Results of the Kolmogorov-Smirnov test applied to verify the statistical agreement between the experimental calibration curves and the three fitting functions.

	Fit function	p value	n*m*$D_{m,n}$	Test result
30 MeV monochromatic	polynomial	0.9999979583	0.0605002	passed
	exponential	0.9997786393	0.6299953	passed
	double exponential	0.999908899	0.4041422	passed
60 MeV monochromatic	polynomial	0.9999487996	0,1325224	passed
	exponential	0.9999762820	0.0901963	passed
	double exponential	0.9999819617	0.0786587	passed
60 MeV modulated	polynomial	0.9999937250	0.0463934	passed
	exponential	0.9998712676	0.2101382	passed
	double exponential	0.9999699324	0,1015546	passed

For all of the nine analyzed cases, the K-S test passed, statistically demonstrating that all three analytical functions can be used for the EBT3 calibration fits. Looking to the K-S statistic parameter

Figure 3. Percentage diference between the experimental calibration curve and the fit function. The three plot report the results for the three irradation conditions and in each plot the predictions obtained with the three studied fitting functions are also superimposed.

d$_{max}$, i.e. the maximum distance between the cumulative curves of the two distributions, it can be noted that the best agreement is obtained in the case of the use of a third-order polynomial fit for the monochromatic 30 MeV beam and the SOBP, while the double exponential function produces the shortest d$_{max}$ for the 60 MeV monochromatic beam. This is also graphically confirmed by figure 3. Even if all the three considered fit functions well reproduce the radiochromic response to the absorbed dose, we decided to adopt the polynomial one as it is the widest adopted in the current literature also for more conventional radiation beams. Table 2 reports, for the three investigated configurations, the values of the polynomial fit parameters and the corresponding errors.

Table 2. Polynomial fit parameters for the three investigated configurations: 30 MeV monochromatic, 60 MeV monochromatic and 60 MeV modulated.

	30 MeV Monochromatic	60 MeV Monochromatic	60 MeV Modulated
p_1	2117 ± 293	3519 ± 807	2424 ± 418
p_2	1241 ± 336	257 ± 6.4	968 ± 411
p_3	626 ± 107	819 ± 315	678 ± 111
p_4	-1.3 ± 8.5	-5.4 ± 26.7	-1.8 ± 7.7

### 4.2 Depth dose curves reconstructions

By adopting the polynomial fit we were able to reconstruct the corresponding depth dose distributions for all three investigated cases. Results are reported in figures 4, 5 and 6. The response of RCF films as a function of the depth in water is directly reported in Gy while the signal of the ionization chamber is normalized to the entrance value of RCF, for the 30 MeV and for the 60 MeV monochromatic cases, and to the value of the RCF in the middle of the spread out Bragg Peak for the 60 MeV modulated case. Total uncertainty on the RCF dose distributions are calculated propagating the errors in the film scan procedure (scanner uniformities, statistical errors in the average pixel values, etc.) and the errors in the fit parameters. The agreement between the two curves resulted always better than 6% except for the 30 MeV case, where RCF underestimates the dose at the peak region up to 18%.

5 Discussion

Scientific literature of the last 10 years reports many studies on the RCF calibration. These works mainly relate to the irradiation with photon beams [9, 25–34] while only a few of them discuss the results on the RCF calibration procedure with proton beams [13, 35–37]. None of them produces a systematic investigation of the most appropriate fitting curve that could be potentially adopted in proton irradiation.

In this paper, we investigated the response of the ETB3 radiochromic films to the absorbed dose released by three different proton beams qualities: 30 MeV and 60 MeV monochromatic and 60 MeV clinical spread-out. The radiochromic response was studied in the dose range of 0.5–15 Gy and three different fitting functions were evaluated. This investigation permitted, for the first time, to find a common calibration procedure and fitting curve for proton beams of different characteristics.
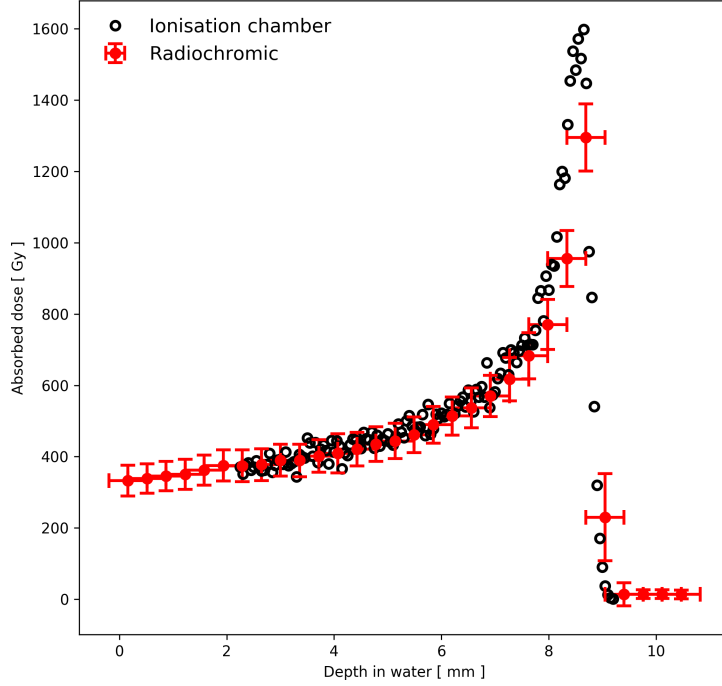
Figure 4. Depth dose distribution of a 30 MeV monochromatic proton beam as measured by a plane-parallel, Markus type ionisation chamber (black circles) compared with the corresponding curve reconstructed using a calibrated stack of radiochromic EBT3 films (red points with errors).

Moreover, the study demonstrated that the use of a single calibration point is sufficient for the reconstructions of the proton beams depth dose distributions with errors below 7%.

6 Conclusion

The RCF appears a promising detector for the use in the absolute dose evaluation of high dose rates beams, where conventional detectors cannot be used. They are dose-rate independent and can be successfully used for the reconstruction of the absolute dose distributions in proton beams of different energies. Given the good results shown in this paper, their use in stack configuration can be also adopted for the reconstruction of the particle energy spectra using energy unfolding techniques. The RCF detectors reported in this paper are being extensively used in the commissioning of the ELIMED laser-driven transport beamline at the ELI-Beamlines facility (Prague, CZ) [8].

Acknowledgments
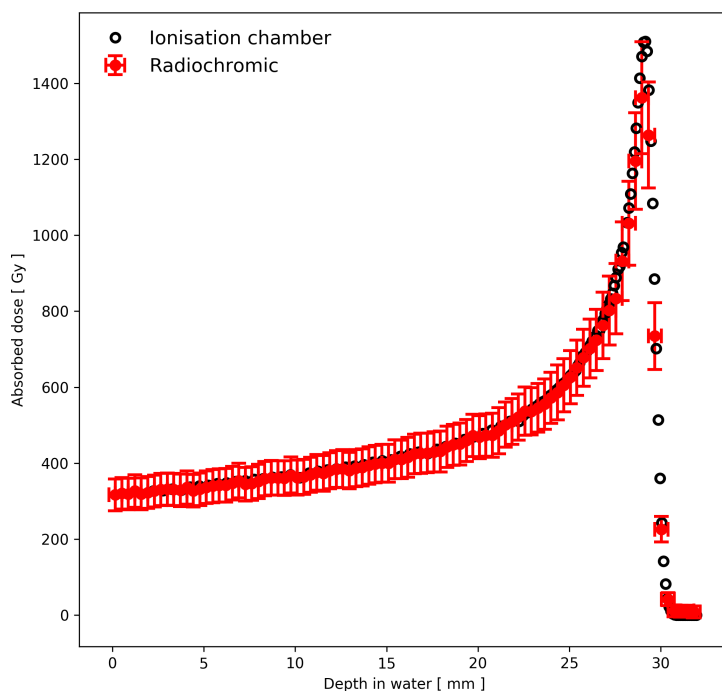
Figure 5. Depth dose distribution of a 60 MeV monochromatic proton beam as measured by a plane-parallel, Markus type ionisation chamber (black circles) compared with the corresponding curve reconstructed using a calibrated stack of radiochromic EBT3 films (red points with errors).
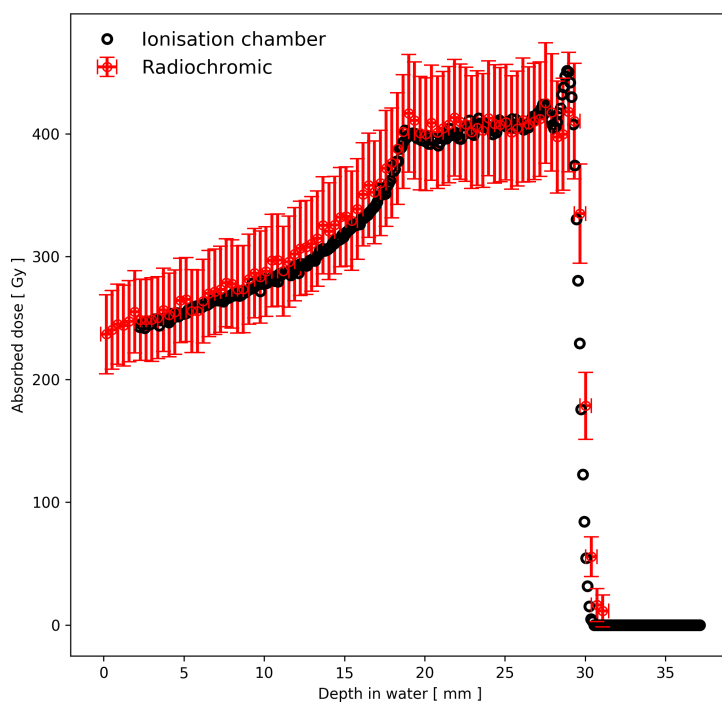
Figure 6. Depth dose distribution of a clinical modulated proton beam as measured by a plane-parallel, Markus type ionisation chamber (black circles) compared with the corresponding curve reconstructed using a calibrated stack of radiochromic EBT3 films (red points with errors).

References

[1] V. Malka, J. Faure, Y.A. Gauduel, E. Lefebvre, A. Rousse and K.T. Phuoc, *Principles and applications of compact laser-plasma accelerators*, *Nature Phys.* **4** (2008) 447.

[2] E. Fourkal, B. Shahine, M. Ding, J.S. Li, T. Tajima and C.-M. Ma, *Particle in cell simulation of laser-accelerated proton beams for radiation therapy*, *Med. Phys.* **29** (2002) 2788.

[3] V. Favaudon et al., *Ultrahigh dose-rate FLASH irradiation increases the differential response between normal and tumor tissue in mice*, *Sci. Transl. Med.* **6** (2014) 245ra93.

[4] M. Jaccard et al., *High dose-per-pulse electron beam dosimetry: Commissioning of the oriatron eRT6 prototype linear accelerator for preclinical use*, *Med. Phys.* **45** (2018) 863.

[5] K. Arakawa et al., *Construction and first year's operation of the JAERI AVF cyclotron*, in *Proceedings of the 13th International Conference on Cyclotrons and their Applications*, edited by G. Dutto and M.K. Craddock, Vancouver, Canada, (1992), p. 119.

[6] R. Cambria, J. Hérault, N. Brassart, M. Silari and P. Chauvel, *Proton beam dosimetry: A comparison between the faraday cup and an ionization chamber*, *Phys. Med. Biol.* **42** (1997) 1185.

[7] S. Lorin, E. Grusell, N. Tilly, J. Medin, P. Kimstrand and B. Glimelius, *Reference dosimetry in a scanned pulsed proton beam using ionisation chambers and a faraday cup*, *Phys. Med. Biol.* **53** (2008) 3519.

[8] D. Margarone et al., *ELIMAIA: A laser-driven ion accelerator for multidisciplinary applications*, *Quantum Beam Sci.* **2** (2018) 8.

[9] S. Devic et al., *Linearization of dose-response curve of the radiochromic film dosimetry system*, *Med. Phys.* **39** (2012) 4850.

[10] K. Krushelnick et al., *Ultrahigh-intensity laser-produced plasmas as a compact heavy ion injection source*, *IEEE Trans. Plasma Sci.* **28** (2000) 1110.

[11] P. Olko, *Advantages and disadvantages of luminescence dosimetry*, *Radiat. Meas.* **45** (2010) 506.

[12] L. Karsch et al., *Dose rate dependence for different dosimeters and detectors: TLD, OSL, EBT films, and diamond detectors*, *Med. Phys.* **39** (2012) 2447.

[13] S. Reinhardt, M. Hillbrand, J.J. Wilkens and W. Assmann, *Comparison of gafchromic EBT2 and EBT3 films for clinical photon and proton beams*, *Med. Phys.* **39** (2012) 5257.

[14] D. Haberberger et al., *Collisionless shocks in laser-produced plasma generate monoenergetic high-energy proton beams*, *Nature Phys.* **8** (2011) 95.

[15] W. McLaughlin, *Film, Dyes and Photographic Systems, Manual on Radiation Dosimetry*, *Marcel Dekker*, New York, U.S.A. (1970).

[16] J. Kosar, *Light Sensitive Systems*, Wiley, New York, U.S.A. (1965).

[17] P. Metcalfe et al., *The Physics of Radiotherapy X-rays from Linear Accelerators*, Medical Physics Publishing, Madison, WI, U.S.A. (1997).

[18] G. Cirrone et al., *A 62-MeV proton beam for the treatment of ocular melanoma at laboratori nazionali del sud-INFN*, *IEEE Trans. Nucl. Sci.* **51** (2004) 860.

[19] N. Givehchi et al., *Online monitor detector for the protontherapy beam at the INFN laboratori nazionali del sud-catania*, *Nucl. Instrum. Meth.* **A 572** (2007) 1094.

[20] G. Cuttone et al., *CATANA protontherapy facility: The state of art of clinical and dosimetric experience*, *Eur. Phys. J. Plus* **126** (2011) 65.

[21] Ashland™, Gafchromic radiotherapy films, (2019),
http://www.gafchromic.com/gafchromic-film/radiotherapy-films/EBT/index.asp.

[22] J. Sorriaux et al., *Evaluation of Gafchromic® EBT3 films characteristics in therapy photon, electron and proton beams*, *Phys. Med.* **29** (2013) 599.

[23] A.M. Gueli et al., *Background fog subtraction methods in Gafchromic® dosimetry*, Phys. Med. **27** (2011) 122e134.

[24] F.J. Massey, *The kolmogorov-smirnov test for goodness of fit*, *J. Am. Statist. Assoc.* **46** (1951) 68.

[25] S. Aldelaijan and S. Devic, *Comparison of dose response functions for EBT3 model GafChromic™ film dosimetry system*, *Phys. Med.* **49** (2018) 112.

[26] R. Dąbrowski, I. Drozdyk and P. Kukołowicz, *High accuracy dosimetry with small pieces of gafchromic films*, *Rep. Pract. Oncol. Radiother.* **23** (2018) 114.

[27] V.C. Borca et al., *Dosimetric characterization and use of GAFCHROMIC EBT3 film for IMRT dose verification*, *J. Appl. Clin. Med. Phys.* **14** (2013) 158.

[28] J.P. Chung, K.Y. Park and B.-C. Kim, *Development of an automated system for radiochromic film analysis*, *Nucl. Instrum. Meth.* **A 922** (2019) 357.

[29] C. Ruiz-Morales, J.A. Vera-Sánchez and A. González-López, *On the re-calibration process in radiochromic film dosimetry*, *Phys. Med.* **42** (2017) 67.

[30] T.B. Dery et al., *Evaluation of Scanner Response with Radiochromic EBT3 Film in Radiation Therapy*, Int. J. Sci. Res. Sci. Technol. (2018) **4** 1646.

[31] L. Menegotti, A. Delana and A. Martignano, *Radiochromic film dosimetry with flatbed scanners: A fast and accurate method for dose calibration and uniformity correction with single film exposure*, *Med. Phys.* **35** (2008) 3078.

[32] S.C. Peet, R. Wilks, T. Kairn, J.V. Trapp and S.B. Crowe, *Technical note: Calibrating radiochromic film in beams of uncertain quality*, *Med. Phys.* **43** (2016) 5647.

[33] D. Lewis, A. Micke, X. Yu and M.F. Chan, *An efficient protocol for radiochromic film dosimetry combining calibration and measurement in a single scan*, *Med. Phys.* **39** (2012) 6339.

[34] A. Micke, D.F. Lewis and X. Yu, *Multichannel film dosimetry with nonuniformity correction*, *Med. Phys.* **38** (2011) 2523.

[35] X.H. Xu et al., *Detection and analysis of laser driven proton beams by calibrated Gafchromic HD-v2 and MD-v3 radiochromic films*, *Rev. Sci. Instrum.* **90** (2019) 033306.

[36] Y. Feng, H.F. Tiedje, K. Gagnon and R. Fedosejevs, *Spectral calibration of EBT3 and HD-v2 radiochromic film response at high dose using 20 MeV proton beams*, *Rev. Sci. Instrum.* **89** (2018) 043511.

[37] D. Krzempek et al., *Calibration of Gafchromic EBT3 film for dosimetry of scanning proton pencil beam (PBS)*, *Radiat. Prot. Dosimetry* **180** (2018) 324.